PCCP

# Surface photochemistry on confined systems: UV-laser-induced photodesorption of NO from Pd-nanostructures on $Al_2O_3$†

**Margarethe Kampling,[a] Katharina Al-Shamery,*‡[a] Hans-Joachim Freund,[a] Markus Wilde,[b] Katsuyuki Fukutani[b] and Yoshitada Murata[b]**

[a] *Fritz-Haber-Institut der Max-Planck-Gesellschaft, Faradayweg 4–6, D-14195 Berlin, Germany*
[b] *Institute of Industrial Science, University of Tokyo, 4-6-1 Komaba, Meguro-ku, Tokyo, 153-8505, Japan*

***Received 6th February 2002, Accepted 15th March 2002***
***First published as an Advance Article on the web 9th May 2002***

UV-laser induced desorption of NO from nanostructured palladium aggregates on an epitaxial alumina support has been studied by means of resonance enhanced multiphoton ionisation (REMPI) to detect desorbing molecules quantum state resolved by Fourier-transform infrared reflection absorption spectroscopy (FT-IRAS), X-ray photoemission spectroscopy (XPS) and thermal desorption spectroscopy (TPD). The size of the Pd-aggregates was systematically varied between 5 Å and 80 Å. Different morphologies were chosen depending on the growth conditions of the aggregates by Pd-atom deposition on the support. The aggregates were either amorphous (deposition at 100 K) or ordered (deposition at 300 K) with the aggregates having a cubooctahedral shape with dominating (111) terraces and a minority of (100) terraces. Adsorption is only similar to single crystal data for aggregate sizes beyond 75 Å. For smaller aggregates NO is bound on on-top sites of palladium. On small amorphous aggregates a substantial amount of NO is weakly bound, which has only been observed for stepped single Pd-crystals. Dissociation of NO occurs at elevated temperatures above 350 K. The system was excited with nanosecond laser pulses at 6.4 eV. In contrast to single crystals, desorption of intact NO molecules has been observed for small aggregates with increasing efficiencies with decreasing aggregate size for aggregate sizes of 80 Å and below. Desorption cross sections vary by at least one order of magnitude. Dominantly the weakly bound species desorbs. REMPI data do not show a strong size dependence. Different models are discussed to explain the data, including the role of local effects of the adsorption site, spill-over to the alumina support or formation of oscillations in electron densities.

## 1. Introduction

The goal of fundamental investigations on surface photochemistry is to get a general insight into the elementary processes of bond breaking and bond making. The use of laser light enables one to study energy redistribution processes preceding bond breaking within an adsorbate in a defined way with respect to energy and time. The concepts developed from these studies contribute to our general understanding of chemical events. A deeper understanding of the relevant processes should finally enable manipulation of chemical reactions.

One possible way of influencing photochemistry in a controlled way is to use confined systems of a defined size. Confined systems like nanostructured surfaces show unique properties as compared with bulk materials. Particular attention in current research has been focussed on metal/oxide interfaces which are of technological importance *e.g.* in catalysis. The main emphasis in surface science studies so far has been put on studies of the catalytic activity and its relation to intrinsic cluster size effects.[1–4]

In the context of surface photochemistry a first theoretical prediction in relation to the particular size dependence of the photochemistry on confined systems has been given by Zhdanov and Kasemo on the enhancement of cross sections of substrate-mediated photoinduced chemical reactions on ultrathin metal films on a semiconductor support.[5] They discussed that energy dissipation will mainly occur in the metal film while the semiconductor minimises inelastic damping of hot electrons. Therefore the electrons will eventually be trapped in the film, generating secondary electrons. From simple calculations Zhdanov and Kasemo predicted that the enhancement factor can easily be a factor of ten and is roughly dependent on the thickness of the metal film and the mean free path with respect to excitation of electron–hole pairs in the metal. Nanometre metal particles with their further unique optical and electronic properties are also suggested to be suitable. A comparable approach has been given in two earlier papers by Gadzuk who developed a theory on resonance-assisted hot electron femtochemistry at surfaces in a solid state tunnel junction composed of metal–insulator–metal substrates.[6,7] The difference between this approach and that of Zhdanov and Kasemo is that the hot electrons are supplied *via* field-induced injection.

The first experimental demonstration of changes of surface photochemistry on confined systems compared to single crystal supports was by Watanabe *et al.*[8] They studied the UV-laser induced C–H activation of methane on Pd-aggregates of sizes smaller than 73 Å, deposited on a thin epitaxial film of alumina grown on NiAl(110). The reaction paths change from a preferential dissociation at large aggregates comparable to single crystal surfaces to preferential desorption from rather small clusters with cross sections changing by at least one order of magnitude. The detection limit for photodissociation of methane on aggregates of ordered structure is around

† Dedicated to Professor Jürgen Troe on the occasion of his 60th birthday.
‡ Permanent address: Carl v. Ossietzky Universität Oldenburg, Fachbereich 9, Postfach 2503, D-26111 Oldenburg, Germany.

$(36.5 \pm 5.5)$ Å. Poisoning effects from the dissociation product $CH_3$ have been observed at much lower concentrations than on single crystal surfaces.

This work stimulated the research summarised in this paper on NO photochemistry on Pd-aggregates deposited on an epitaxial alumina support. The goal was to get a detailed insight into the dominant processes governing the photostimulated desorption by using quantum state resolved methods to detect energy redistribution within desorbing molecules. The presented data are the first quantum state resolved measurements on nanostructured surfaces. The excitation energy of 6.4 eV was below the band gap of the alumina. Cross sections of laser induced desorption from metals are normally rather small if detectable at all.[9] While no detectable desorption has been observed for nanosecond laser excitation of NO adsorbed on a Pd-single crystal surface, desorption has been reported for femtosecond laser excitation.[10] In the following it will be shown that desorption can also be observed from nanosized Pd-aggregates using nanosecond lasers, with increasing efficiency for decreasing aggregate sizes. A detailed discussion of the binding of NO on the aggregates will also be given as it is substantially different from adsorption at bulk crystals. The latter is also relevant for discussions of the functioning of catalysts.

## 2. Experimental set-up

The experiments were carried out in a UHV-chamber which has been described in detail elsewhere.[11] The system was equipped with LEED (low energy electron diffraction), SPA-LEED (spot profile analysis-LEED), AES (Auger electron spectroscopy), XPS (X-ray photoelectron spectroscopy), XAES (X-ray Auger electron spectroscopy) and a TPD facility. Furthermore additional laser experiments combined with infrared spectroscopy have been performed in Japan.[12] The FTIR-spectra were recorded with 2 $cm^{-1}$ resolution. A NiAl(110) crystal was connected with tantalum rods to a sapphire attached to a copper liquid nitrogen reservoir which allowed cooling to 100 K. The sample temperature was controlled by a chromel–alumel thermocouple spot welded to the side of the crystal. Several cycles of neon ion bombardment and annealing were necessary to clean the crystal from contamination. An epitaxial film of $Al_2O_3$ of 5 Å thickness was obtained by oxidising the cleaned crystal in an atmosphere of $10^{-6}$ Torr of oxygen at 600–800 K and annealing the oxide to 1000 K. Prior to each measurement the sample was freshly sputtered and oxidized.

Palladium atoms were evaporated from an evaporation oven with calibration of the coverage with a microbalance and XPS. The cluster sizes and island densities were obtained from SPA-LEED measurements which confirmed data reviewed in the literature.[13] Under the experimental conditions presented, amorphous aggregates with average sizes between 5 Å and 70 Å have been obtained by depositing Pd at 100 K. The island density ranges from $2.5 \times 10^{13}$ $cm^{-2}$ to $2 \times 10^{12}$ $cm^{-2}$.[13] Ordered Pd-aggregates of sizes varying between 30 Å and 80 Å have been obtained by deposition of Pd at 300 K. They exhibit cubooctahedral shapes with a majority of (111) terraces and a minority of (100) terraces.[14] The island density ranges from $2 \times 10^{11}$ $cm^{-2}$ to $1.25 \times 10^{12}$ $cm^{-2}$.[13] Typical error bars are for example for an average aggregate size of 45 Å in the range of 15 Å.

A saturation coverage of a monolayer of NO was dosed prior to the experiments *via* a pinhole doser system. NO molecules were desorbed by pump laser pulses of a broad band excimer laser (Lambda Physik EMG 200) run at 6.4 eV with normal incidence on the surface. The laser fluence was typically 1 mJ $cm^{-2}$ per pulse in most of the experiments with a pulse length of 15 ns. The desorbing molecules were detected in the gas phase using the well known $(1 + 1)$ REMPI scheme (resonance enhanced multiphoton ionisation) *via* the A $^2\Sigma$-state.[15] Detection followed the desorption pulse after a well defined time delay at a distance of 32 mm parallel to the surface with an excimer laser (XeCl, Lambda Physik LPX 205 i cc) pumped tunable dye laser (Lambda Physik LPD 3002). The ions were detected perpendicular to the desorption and detection laser beam direction with a repeller electrode, a short drift tube, microchannel plates and a phosphor screen.

To conduct photodesorption experiments at higher NO coverages background gas dosing was necessary in order to redose a larger number of molecules between the desorption laser pulses. Therefore the detection laser was operated at twice the desorption laser frequency (2 Hz) and the background signal due to the gas phase NO recorded between the desoption pulses was then easily subtracted using a boxcar integrator.

## 3. Results

NO adsorption at nanostructured metal particles turned out to be substantially different from that at single crystal surfaces. As no systematic data on well defined systems within the size regime relevant for the experiments presented have been documented before the characterisation of the adsorbate system has to be discussed first, before the results on laser induced desorption can be tackled.

### 3.1 NO adsorption on $Pd/Al_2O_3$

NO adsorption was studied with TPD, IRAS and XPS and will be compared to single crystal studies. NO adsorbs intact on the Pd aggregates at 100 K. The data will be presented in the first part of this section. Depending on the aggregate size NO can be thermally dissociated when heating the surface to temperatures above 350 K, as will be discussed in a following section. Irradiation with UV-laser light does not lead to photodissociation products as is apparent from IRAS, XPS and TPD.

On the alumina support itself NO only adsorbs at defect sites at the working temperature of 100 K during the laser experiments. This is apparent from Fig. 1, which shows the TPD spectra of NO adsorbed on the pure alumina support as a function of coverage recorded with a linear temperature ramp of 0.5 K $s^{-1}$. The recorded $m/z$ is 30. The monolayer desorption peaks at 64 K. This corresponds to an adsorption

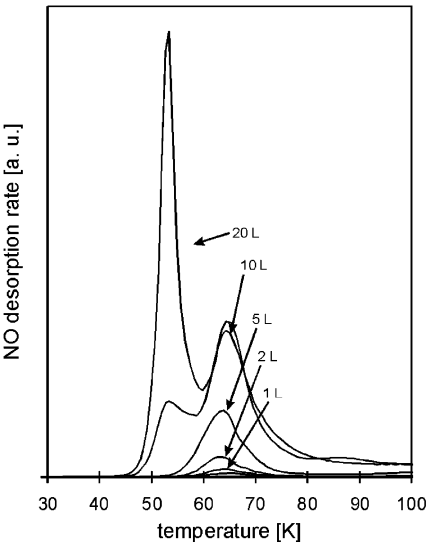


**Fig. 1** TPD spectra of NO adsorbed on the pure alumina support as a function of coverage (linear temperature ramp of 0.5 K $s^{-1}$), $m/z = 30$.

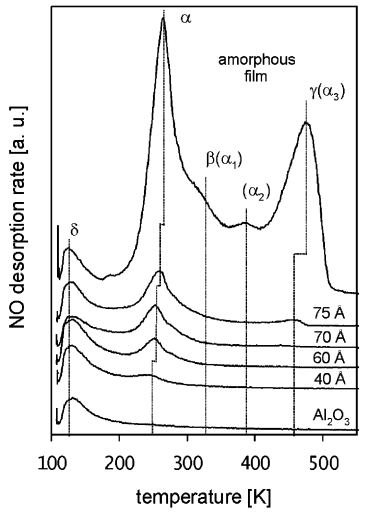


**Fig. 2** TPD data of saturation coverages of NO adsorbed on ordered Pd aggregates, sizes ranging from 40 Å to 75 Å [total amount of Pd deposited according to microbalance: 1.5 Å (aggregate size 40 Å); 3.5 Å (aggregate size 60 Å); 7 Å (aggregate size 70 Å); 14 Å (aggregate size 75 Å)] and on an amorphous Pd film on an alumina support (total amount of Pd deposited: 50 Å); linear temperature ramp of 0.5 K $s^{-1}$, $m/z = 30$.

energy of 0.18 eV according to a Redhead analysis assuming a frequency factor of $10^{13}$ $s^{-1}$. A second peak is observed at 54 K and can be attributed to the formation of further layers after saturation of the monolayer. A peak with a maximum at 100 K with an area of *ca.* 1% of a monolayer can be attributed to desorption from defect sites.

Fig. 2 shows TPD data of saturation coverages of NO adsorbed on ordered Pd aggregates with sizes ranging from 40 Å to 75 Å and on a polycrystalline Pd film on an alumina support. The temperature ramp is 0.5 K $s^{-1}$ starting at 100 K. A feature between 100 K and 120 K can be attributed to desorption from defect sites on alumina as mentioned above (marked δ in Fig. 2). For aggregates below a size of 75 Å only one desorption peak at 246–264 K can be observed, corresponding to binding energies of 0.70–0.75 eV. In contrast to single crystals there are no high temperature features above 350 K. This may be attributed to thermally induced dissociation with a subsequent recombinative desorption of $N_2$ and $N_2O$ species during the heating process, as will be discussed further below. The relatively low TPD intensity of the small Pd-aggregates compared to the polycrystalline film has to be attributed to the low overall surface area (of the order of a few percent with respect to the alumina surface for the smallest aggregates).

The TPD spectrum from the amorphous film is complex and resembles single crystal data of Pd(111) in view of the dominating desorption maxima as well as their intensity distributions. Therefore we ascribed the relevant desorption maxima in Fig. 2 with α, β and γ reminiscent of the Pd(111) surface. A further feature around 380 K may be attributed to a species from the minority of Pd(100) facets (known as $\alpha_2$ species). The maxima of $\alpha_1$ and $\alpha_3$ from the Pd(100) facets overlap with the β and γ-species of the Pd(111) facets. Table 1 summarises the NO desorption maxima of the different preparations of ordered Pd aggregates. Table 2 is an overview of literature data found for Pd single crystals of different orientations. In combination with LEED and HREELS (high resolution electron energy loss spectroscopy) the complex TPD data of NO from palladium single crystals have been interpreted as being due to repulsive interactions between NO molecules adsorbed on single (α species on Pd(111)) and more strongly bound higher coordinated sites (β and γ species on Pd(111)).[16–18]

Fig. 3(a) and (b) show TPD data from amorphous palladium aggregates on alumina. Besides a single desorption peak around 260 K no desorption peaks at more elevated temperatures are observable for aggregates of 55 Å and smaller. Again this may be attributed to NO dissociation above 350 K. Further weakly bound species are visible as a shoulder of the desorption feature from bare alumina near 80 K and a maximum at 140 K which do not have any match to single crystal data. As NO multilayer adsorption occurs at temperatures below 55 K they may tentatively be attributed to adsorption at defects, kinks and edges which are present to a large extent on the amorphous Pd-aggregates. The high density of non-regular adsorption sites, a different polarizability of the aggregates with respect to the bulk material and the strong repulsive interaction of adsorbed NO molecules may explain why this weak adsorption feature is predominant for the amorphous aggregates. While, under UHV conditions, full saturation coverage only occurs below 85 K, nevertheless this species may be important under elevated pressures, as used in heterogeneous catalysis. Our laser experiments have been performed with a permanent back ground dosing at 100 K. Under these conditions species with a finite residual time on the surface may also play a role in the experiments presented.

Fig. 4(a) and (b) show IRAS spectra of NO adsorbed on ordered Pd aggregates on alumina for an average aggregate size of 80 Å within a frequency range of the NO stretching vibration. Fig. 4(a) is a series of spectra taken for different coverages of NO adsorbed at 100 K. Fig. 4(b) is a series of spectra taken of a saturation coverage of NO adsorbed at 100 K and heated to the temperature indicated. Depending on the probe temperature and the NO coverage three main features can be identified. At low coverages a peak at 1535 $cm^{-1}$ appears, shifting to 1605 $cm^{-1}$ with increasing coverage. This feature belongs to the most strongly bound species, as apparent from the temperature behaviour. A second feature is observable at 1665 $cm^{-1}$, shifting to 1685 $cm^{-1}$ at higher coverages, which also belongs to a stronger bound species. At high coverages only one feature at 1750 $cm^{-1}$, shifting to 1760 $cm^{-1}$ is present in the IRAS spectra. This peak belongs to adsorption sites which disappear above 300 K. Note that no infrared signal could be detected for NO on the pure alumina. Table 3 summarises HREELS data from the literature obtained for palladium single crystals of different orientations.

**Table 1** NO desorption maxima of the different preparations of ordered Pd aggregates (saturation coverage at 100 K, heating rate: 0.5 K $s^{-1}$)

| | | Desorption temperature | | |
|---|---|---|---|---|
| Preparation | Diameter of aggregates | α | β | γ |
| 50 Å/300 K | — | 264 K (0.75 eV) | 322 K (0.93 eV) | 476 K (1.39 eV) |
| 14 Å/300 K | 75 Å | 260 K (0.74 eV) | — | 462 K (1.34 eV) |
| 7 Å/300 K | 70 Å | 254 K (0.73 eV) | — | — |
| 3.5 Å/300 K | 60 Å | 252 K (0.72 eV) | — | — |
| 1.5 Å/300 K | 40 Å | 246 K (0.70 eV) | — | — |

**Table 2** Overview of literature data of desorption maxima found for Pd single crystals of different orientations

| Surface | Desorption temperatures | | | References |
|---|---|---|---|---|
| Pd(111) | 260 K ($\alpha$) | 280 K ($\beta$) | 510 K ($\gamma$) | 16–18 |
| Pd(100) | 290 K ($\alpha_1$) | 410 K ($\alpha_2$) | 535 K ($\alpha_3$) | 19 |
| Pd(110) | 260 K | 350 K | 480 K | 20,21 |

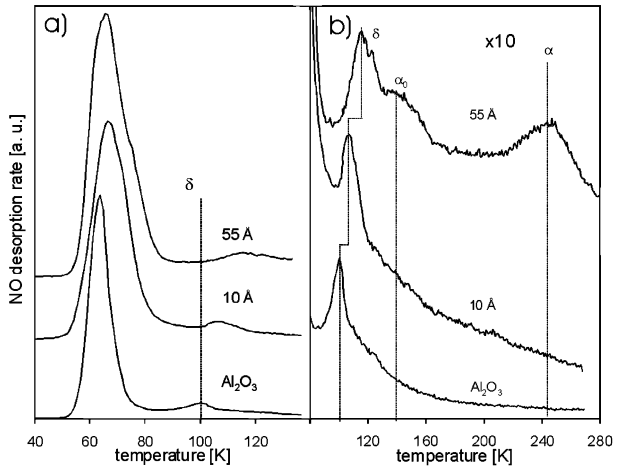


**Fig. 3** TPD data of 10 L NO deposited at 30 K from amorphous palladium aggregates on alumina with an average size of 10 Å (total amount of Pd deposited: 0.5 Å according to microbalance) and 55 Å (total amount of Pd deposited: 10 Å)); linear temperature ramp of 0.5 K $s^{-1}$, $m/z = 30$. (a) Overview, (b) details of (a) enlarged.

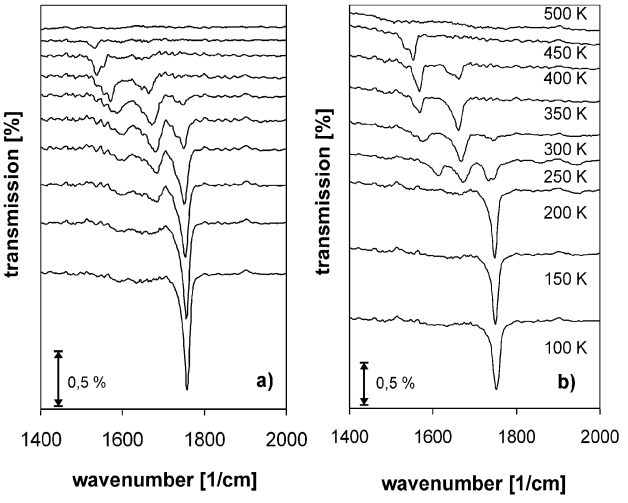


**Fig. 4** IRAS spectra of NO adsorbed on ordered Pd aggregates on alumina for an average aggregate size of 80 Å (total amount of Pd deposited: 20 Å according to microbalance). (a) Series of spectra taken for different coverages of NO adsorbed at 100 K. (b) Series of spectra taken of a saturation coverage of NO adsorbed at 100 K and heated to the temperature as indicated.

The adsorption behaviour on the larger ordered Pd aggregates can be compared to the observation on the stepped Pd(112) single crystal by Ramsier *et al.*[22] The Pd(112) surface consists of terraces of (111) character (3 atoms wide) and monoatomic (001) steps. At low coverages they observe with HREELS a single peak at 1522 $cm^{-1}$ which they attribute to adsorption on higher coordinated sites on the regular terraces. A growing second feature in the HREEL spectra around 1640 $cm^{-1}$ is interpreted as due to a sequential population of positions at the (001) step edges at intermediate coverages. At large coverages a single peak at 1750 $cm^{-1}$ attributed to on-top positions is visible. In recent findings, which are reviewed by Brown and King,[24] a rough assignment of NO stretching vibrational frequencies is given as follows: atop NO 1700–1850 $cm^{-1}$, 2-fold NO 1640–1710 $cm^{-1}$ and 3-fold NO 1450–1645 $cm^{-1}$. Strong shifts of the vibrational frequencies of 3-fold NO are related to the occurrence of NO in close-lying fcc and hcp positions which are areas of elevated adsorbate density and thus a cause of strong coupling.

In the IR, according to Wolter *et al.*, only vibrations of the top terraces and upper edges show substantial intensities due to infrared selection rules.[25] We therefore interpret the IR data as follows. For large ordered aggregates first higher coordinated positions on regular terrace sites are occupied (1535–1605 $cm^{-1}$) which are likely to be isolated 3-fold hollow sites. The occurrence of absorptions around 1665–1685 $cm^{-1}$ could be due either to occupation of edge sites and kinks or to the formation of adsorption sites with higher local adsorbate density. A finite conclusion about the exact site cannot be drawn from the IR-spectra alone. At the end only on-top positions are covered (1750–1760 $cm^{-1}$). For this type of binding no distinction can be made between regular terrace sites and defect or edge sites.

Fig. 5(a) and (b) show infrared spectra of NO on amorphous palladium aggregates of an average size of 10 Å. Again Fig. 5(a) shows the coverage dependence and Fig. 5(b) shows the temperature dependence of the NO stretching vibration. Only one feature is visible at 1760 $cm^{-1}$ when looking at the coverage dependence. Nearly half of the intensity of this feature is lost when heating the surface to 200 K. At 250 K a minor feature at 1650 $cm^{-1}$ appears. Above 300 K no IR spectra could be detected for NO. According to the previous discussion the peak at 1760 $cm^{-1}$ may be attributed to adsorption on regular on-top sites in accordance with Pd(111) data by Bertolo *et al.*[18,26,27] Defect and edge sites show similar spectra and can only be identified by the temperature behaviour of the overall spectrum.

Fig. 6(a) and (b) show the aggregate size dependence of the NO stretching vibration at saturation coverage for amorphous and ordered aggregates. There is only one major feature visible for all aggregates. Only for rather small aggregates, containing a couple of tens of atoms, is an asymmetry and broadening of the peak visible, which is normally indicative of an increasing density of defect states. Intensity transfer from lower frequencies towards higher frequencies explains the still rather large intensity of the absorption at 1760 $cm^{-1}$.[28]

**Thermal induced dissociation.** Though no NO dissociation occurred during the laser experiments, NO dissociation is relevant when thermally heating the system above 350 K. As this is the reason why quantification of laser desorption with TPD is difficult a short discussion of thermal dissociation will follow. Besides intact thermal desorption of NO molecules, a strongly Pd-aggregate size dependent desorption of reaction products like $N_2$ and $N_2O$ can be observed. This is seen in Fig. 7 showing a TPD-spectrum of different masses (temperature ramp: 0.5 K $s^{-1}$) for a representative sample of an aggregate size of 70 Å grown at 100 K. The ratio of the reaction product $N_2$ to undissociated NO increases with increasing aggregate size up to 80 Å for both types of aggregates (*i.e.* amorphous and ordered). Up to approximately 15–20% of an initial saturation coverage dosed at 100 K desorbs recombinatively as $N_2$ for the largest ordered aggregate investigated here, of 80 Å. A similar percentage remains on the surface as atomic nitrogen. This increase is related to a saturation coverage of NO deposited at 100 K including weakly bound species. The reaction is thermally induced, as can be seen from XPS data at temperatures above 350 K. Fig. 8 shows the N 1s signal of a series of spectra, taken

**Table 3** Vibrational frequencies obtained for palladium single crystals of different orientations and for Pd-aggregates of different sizes (in parentheses: total amount of Pd deposited)

| Surface | Species | Vibrational frequency/cm$^{-1}$ | Reference |
|---|---|---|---|
| Pd(111) | Higher coordination site | 1522–1619 | 18 |
| | | 1535–1600 | 22 |
| | On-top (α) | 1757 | 18 |
| | | 1750 | 22 |
| | NO-dimer | 1789 | 18 |
| Pd(112) | Pd(111)-terrace, higher coordination site | 1522–1540 | 22 |
| | Pd(111)-terrace, on-top | 1738 | 22 |
| | Pd(001)-step | 1645 | 22 |
| Pd(100) | Bridge | 1505 | 19 |
| | | 1498 | 23 |
| | On top | 1660–1720 | 19 |
| | Dimer | 1660–1684 | 23 |
| Pd(110) | Bridge | 1505–1536 | 20 |
| | On top | 1631–1688 | 20 |
| | Dimer | 1720–1734 | 20 |
| 10 Å diameter, amorphous | | 1760 (shoulder at higher coverage: 1745) | This paper |
| 80 Å diameter, ordered | | 1535–1605 | This paper |
| | | 1665–1685 | |
| | | 1750–1760 | |

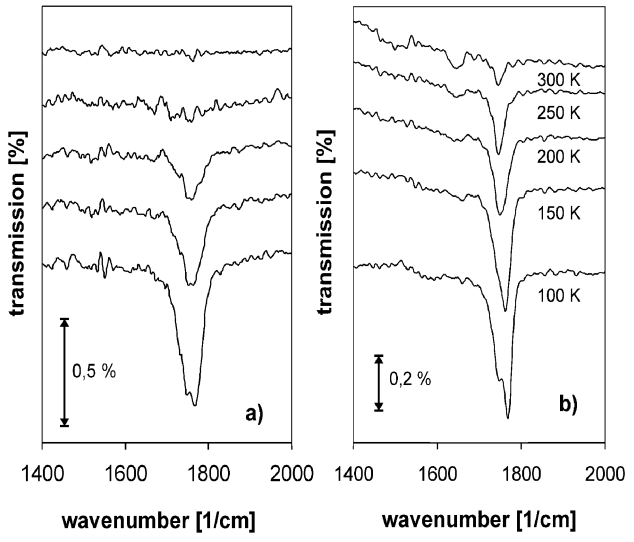


**Fig. 5** IRAS spectra of NO adsorbed on amorphous Pd aggregates on alumina for an average aggregate size of 10 Å (total amount of Pd deposited: 0.5 Å according to microbalance). (a) Series of spectra taken for different coverages of NO adsorbed at 100 K. (b) Series of spectra taken of a saturation coverage of NO adsorbed at 100 K and heated to the temperature indicated.

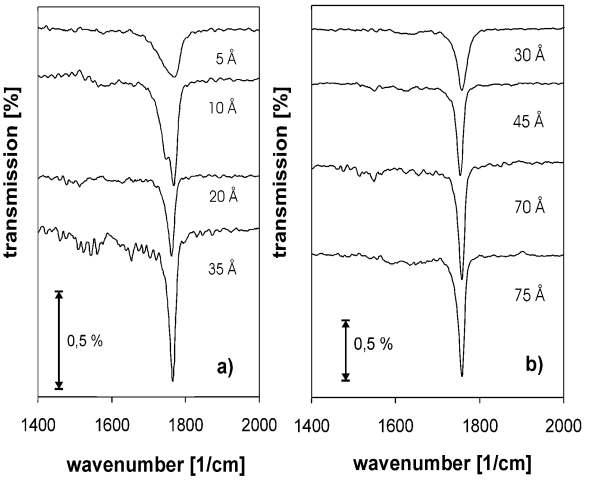


**Fig. 6** Aggregate size dependence of the NO stretching vibration at saturation coverage for (a) Amorphous aggregates [total amount of Pd deposited according to microbalance: 7 Å (aggregate size 35 Å); 2 Å (aggregate size 20 Å); 0.5 Å (aggregate size 10 Å); 0.2 Å (aggregate size 5 Å)] and (b) ordered aggregates [total amount of Pd deposited according to microbalance: 20 Å (aggregate size 75 Å); 10 Å (aggregate size 70 Å); 2 Å (aggregate size 45 Å); 0.5 Å (aggregate size 30 Å)].

as a function of temperature, of an initial saturation coverage of NO on amorphous aggregates with an average size of 80 Å. Small amounts of atomic oxygen cannot be discerned in XPS from the alumina support signal. However palladium is known to be able to store larger amounts of subsurface oxygen.[22,29]

No species other than NO are observed in the IR spectra taken as a function of temperature. This indicates that possible IR active species desorb during formation. However, some atomic residuals of nitrogen remain on the surface, as is apparent in the XPS data.

The situation thus resembles findings on NO dissociation at stepped Pd(112) surfaces.[22] Dissociation occurs at the steps and results in products such as NO, $N_2$ and $N_2O$.[22] No $O_2$ or $NO_2$ was detected. This implies a disproportionation reaction which favours the thermal desorption of N-containing species and solvation of the remaining oxygen within the palladium.

NO dissociation on Pd particles on an $\alpha$-$Al_2O_3$ has been reported by Cordatos *et al.* for particles with sizes larger than 50 Å.[30] They observed a decrease in dissociation efficiency with increasing aggregate size. Their TPD data were obtained for NO deposition at 300 K. Therefore their observation has to be related to the strongly bound species alone. The statement in our paper refers to a full saturation coverage of NO adsorbed at 100 K, including a large amount of weakly adsorbed species. Work on Pd(112) single crystals by Ramsier *et al.* has shown that the thermally induced dissociation of NO is more efficient at lower coverages at the stepped surface[22] which could also explain discrepancies between our observations and those of Cordatos *et al.* Furthermore the size regime is different in the two experiments. Further investigations on NO dissociation, including its coverage dependence, are currently under way to get a more detailed picture of the dissociation process and will be published elsewhere together with a more detailed discussion of the adsorption data.

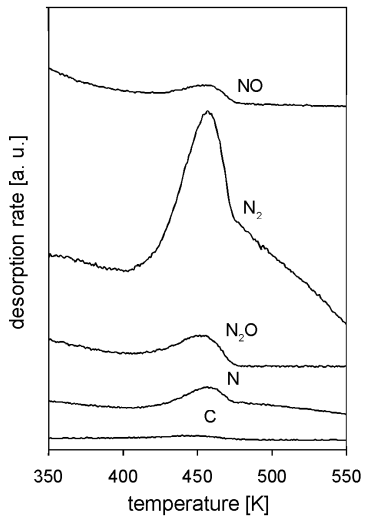


**Fig. 7** TPD-spectra of a saturation coverage of NO on an amorphous aggregate of 70 Å (total amount of Pd deposited according to microbalance: 14 Å), $m/z = 12$ (C), $m/z = 14$ (N), $m/z = 44$ ($N_2O$), $m/z = 28$ ($N_2$) and $m/z = 30$ (NO)); linear temperature ramp of 0.5 K $s^{-1}$.

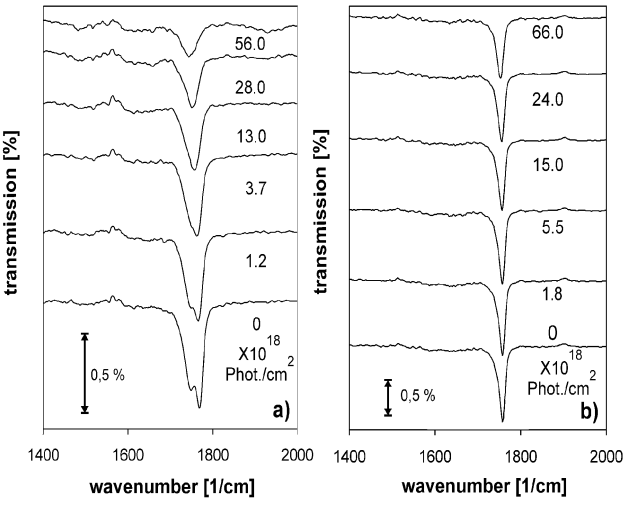


**Fig. 9** (a) IRAS data for a series of different laser exposures of an initial saturation coverage of NO adsorbed on 10 Å sized amorphous aggregates (total amount of Pd deposited: 0.5 Å); $h\nu = 6.4$ eV. (b) IRAS data for a series of different laser exposures of NO adsorbed on a large ordered aggregate of 80 Å diameter (total amount of Pd deposited: 20 Å); $h\nu = 6.4$ eV.

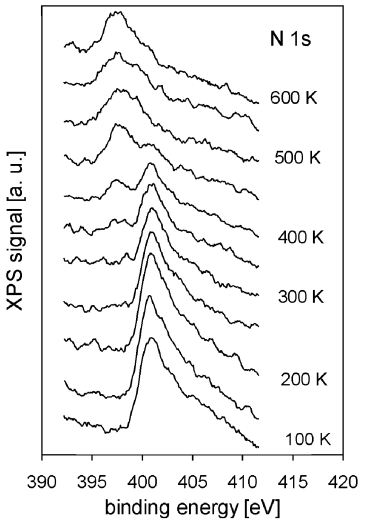


**Fig. 8** XPS spectra, N 1s signal of an initial saturation coverage of NO on amorphous aggregates with an average size of 80 Å (total amount of Pd deposited: 20 Å) taken as a function of temperature in increments of 50 K.

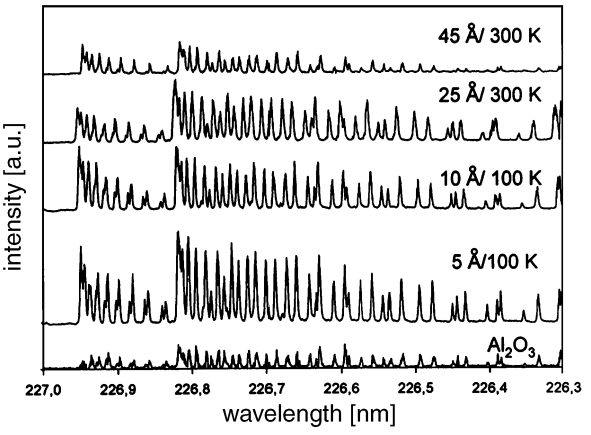


**Fig. 10** Overview of part of the (1 + 1)-REMPI-spectra of NO (*via* the A $^2\Sigma$-state) desorbing from the defect sites of the pure $Al_2O_3$ and from different sized palladium aggregates [total amount of Pd deposited according to microbalance: at $T = 100$ K: 0.2 Å (aggregate size 5 Å); 0.5 Å (aggregate size 10 Å); at $T = 300$ K: 0.5 Å (aggregate size 25 Å); 2 Å (aggregate size 45 Å)]; $v'' = 0$, $v = 1000$ m $s^{-1}$, $h\nu = 6.4$ eV; the part of the spectrum depicted shows part of the transitions from the $^2\Pi_{3/2}$ state.

### 3.2 UV-laser induced desorption of NO

NO was desorbed, starting with a saturation coverage, by exciting the surface with UV-laser light at 193 nm (6.4 eV). Desorption was followed by REMPI during the course of the laser experiment, by IRAS after exposing the surface to a defined number of photons and by TPD after finishing the irradiation. Fig. 9(a) shows, as an example, the IRAS data for a series of different laser exposures of NO adsorbed on 10 Å sized amorphous aggregates. Fig. 9(b) shows the NO stretching vibration spectra when irradiating NO on a large ordered aggregate of 80 Å diameter. While the infrared spectrum of the small aggregate is strongly affected by laser irradiation the effect is much smaller on the large ordered Pd particle. The examples shown are the extreme cases. Generally an increase of the desorption efficiency with decreasing aggregate size is found for both amorphous and ordered aggregates. As IR intensities can be strongly influenced by diverse coupling processes, by a change of polarisability of the small aggregates, and as only NO molecules on the top terraces and edges show relevant IR intensities due to IR selection rules, no reliable quantitative statements can be extracted from the pure IR data. But TPD and REMPI measurements confirm the above observations, as will be discussed further below.

Fig. 10 is an overview of part of the REMPI-spectra of NO desorbing from the defect sites of the pure $Al_2O_3$ and from different sized palladium aggregates of NO in the vibrational ground state. *Via* background dosing a constant concentration was kept on the surface. The desorbing molecules have an average velocity of 1000 m $s^{-1}$ as the spectra have been recorded at a fixed distance from the surface and a fixed time delay. The REMPI signal scaled linearly for all measured quantum states for desorption laser pulses between 0.1 mJ $cm^{-2}$ and 1 mJ $cm^{-2}$. The data can be analysed by assuming a simple Maxwell–Boltzmann distribution. The related rotational temperatures are summarised in Table 4. They are clearly much larger than the surface temperature including

**Table 4** Rotational temperatures for NO desorption of different sized Pd-aggregates after UV-laser excitation at 6.4 eV from Boltzmann analysis of REMPI spectra recorded for $v = 1000$ m s$^{-1}$ (vibrational ground state)

| | Preparation | | | | |
|---|---|---|---|---|---|
| | 0.2 Å/100 K | 0.5 Å/100 K | 0.5 Å/300 K | 2 Å/300 K | $Al_2O_3$ |
| Aggregate diameter | 5 Å | 10 Å | 25 Å | 45 Å | |
| $P_{22} + Q_{12}$[a] branch, $^2\Pi_{3/2}$ | 426 K | 439 K | 432 K | 269 K | 475 K |
| $P_{21} + Q_{11}$[b] branch, $^2\Pi_{1/2}$ | 497 K | 626 K | 490 K | 411 K | |

[a] Analysed for $E_{rot} < 800$ cm$^{-1}$. [b] Analysed for $E_{rot} < 1200$ cm$^{-1}$.

the temperature jump from laser irradiation. This indicates that desorption is initialised by a non-thermal process. Except for the first 6 rotational quantum states, which show steeper slopes, the Maxwell–Boltzmann analysis results in linear plots. The large error bars (of the order of ±50 K or even larger) have several causes. First, the intensities of the REMPI signals are smaller than usually found for comparable cross sections on single crystals. The reason for this is that the small Pd-aggregates only cover a small percentage of the alumina support while desorption from the large aggregates with a larger surface area exhibits much smaller desorption cross sections.

Vibrationally excited NO can also be observed, further ruling out thermally induced processes. However, the poor signal to noise ratio within these spectra did not allow an accurate determination of the vibrational temperatures.

After heating the surface to 200 K the laser desorption experiment was repeated, this time without redosing *via* a background pressure of NO. From the smallest aggregates (5–30 Å) desorption can still be observed, though the overall signal is much smaller. For larger aggregates no desorption was detectable. The final state distributions are similar to the preparation including the weakly bound species. Though the overall intensity is much smaller the depletion shows a similar behaviour to that of a coverage including weakly bound species. Within TPD a general decrease of the α species can be noted for the experiments in which the probe was annealed to 200 K prior to the laser experiment. Though the data point towards involvement of a diffusion process, neither IR not TPD allow final conclusions.

Fig. 11 shows a selected number of velocity flux distributions for ordered Pd-aggregates with an average size of 45 Å for the $^2\Pi_{1/2}$ ($Q_{11}$-transitions in the REMPI spectrum) and the $^2\Pi_{3/2}$ states ($P_{22}$-transitions) of desorbing NO. The single points shown within the spectrum are calculated from averaged data, each taken at a fixed time delay between pump and probe laser. The thus obtained time of flight distributions have been changed into velocity flux distributions as is described in the literature.[11] The coverage was kept constant *via* background dosing. The spectra were normalised to 1 in order to show differences more clearly. Because of a poor signal to noise ratio the velocity flux distributions of the chemisorbed species alone could not be recorded properly. The velocity flux distributions are non-Maxwell–Boltzmann distributions, consisting of a slow and a fast component. The slow component is dominant for low rotational excitation, particularly for small aggregates. The fast component dominates rotationally excited states and is slightly more apparent at larger aggregates. For the Maxwell–Boltzmann analysis of a rotational spectrum discussed above the overall intensity within the rotational state at a fixed velocity is relevant for extracting a rotational temperature. As the spectra have been recorded at $v = 1000$ m s$^{-1}$ the rotational temperatures reflect the rotational temperature of the fast component, if low rotational quantum states are not accounted for. Whether the two components belong to two different channels or are intrinsic from the desorption process (*i.e.* result from the potential energy surfaces involved) can only be revealed by theoretical calculations.

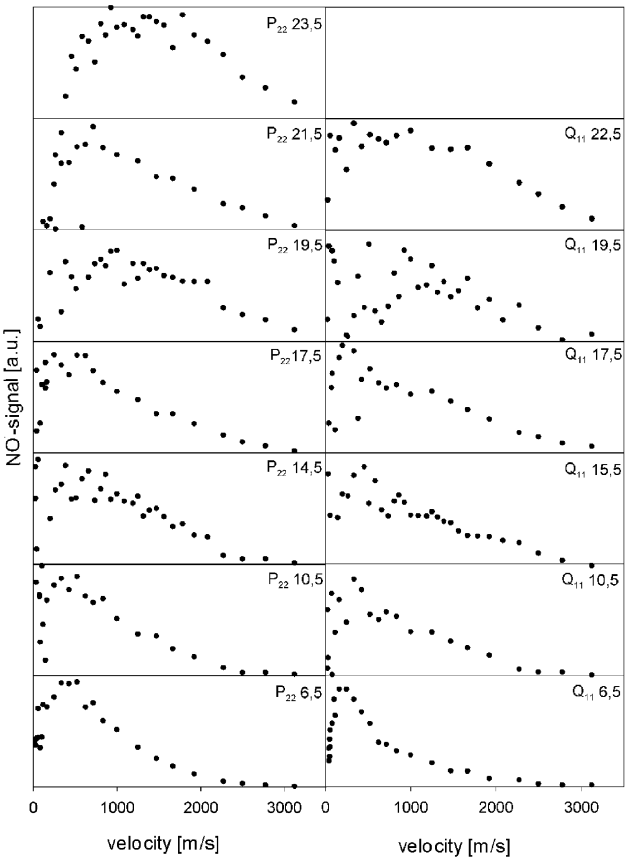


**Fig. 11** A selected number of velocity flux distributions as a function of rotational quantum number of desorbing NO from Pd-aggregates deposited at 300 K with an average size of 45 Å for the $^2\Pi_{1/2}$ ($Q_{11}$ transitions within the REMPI spectra) and the $^2\Pi_{3/2}$ states ($P_{22}$ transitions).

One final remark has to be made with respect to quantification of the desorption efficiencies. Extracting cross sections from IRAS measurements is not advisable as only part of the NO species are IR-active. The TPD data are difficult to analyse, particularly with respect to the weakly bound species, due to the broad background from $Al_2O_3$ defect states and because of aggregate size dependent thermally induced dissociation, which is suspected to be coverage dependent. To analyse the decay of REMPI-intensities the palladium aggregates were fully covered with NO. The decay of the REMPI signal was recorded as a function of laser pulses impinged on the surface. Assuming a simple exponential decay results in cross sections between $10^{-18}$ cm$^2$ for amorphous clusters of 10 Å diameter and $2 \times 10^{-19}$ cm$^2$ for ordered aggregates of 45 Å diameter. Minority species with rather large cross sections might

dominate the REMPI-intensities. However, in view of the strong decrease in the weakly bound species observed in the IR measurements this cross section might be attributed to the weakly bound site.

## 4. Summary and conclusions

For the first time we have shown that molecules can be desorbed with UV-nanosecond laser pulses from metal surfaces when reducing the crystallite size to the nanometre size regime, even for systems for which no desorption is detectable from single crystal surfaces. Elaborate quantum state resolved measurements on the UV-laser induced desorption of NO from palladium aggregates on epitaxial alumina give insight into the desorption process. The desorption has been systematically studied as a function of aggregate size and morphology for defined nanostructures of Pd-aggregates with average sizes between 5 Å and 80 Å. Amorphous and ordered aggregates have been investigated. Deposition of palladium at 100 K leads to highly dispersed aggregates with an amorphous structure.[1,13] Cubooctahedral ordered structures with mainly (111) terraces and a minority of (100) terraces are obtained when growing the aggregates at 300 K.[1,13]

Beside the presentation of laser induced desorption a detailed description of the NO adsorption is discussed in the paper as NO adsorption at nanosized Pd-aggregates differs substantially from adsorption at single crystal surfaces. This finding is of great importance for understanding elementary processes in heterogeneous catalysts used, for example, in car exhausts.

The adsorption of NO on single crystals is dominated by the strong repulsive interaction of NO. On single crystals NO adsorbs predominantly at higher coordinated sites for smaller coverages changing to more weakly bond on-top sites for larger coverages. Sudden changes in the adsorption energy result from changes in the distances between NO molecules and are connected to the highly repulsive interaction of neighbouring molecules.

It is well known that charge density variations occur at step sites of metals which extend into the terrace regions.[31–34] On a nanoparticulate metal the whole terrace might thus be affected, which could lead to drastic changes of properties compared with low index surfaces. Also the polarisability is known to decrease with respect to single crystals.[8] Therefore it is not surprising that adsorption on nanoparticulate metals can differ from adsorption at single crystals.

On Pd-aggregates NO only bonds to on-top sites with binding energies similar to the on-top species on low index single crystal surfaces (0.72 eV $\pm$0.03 eV) on all aggregates investigated smaller than 75 Å. Besides this known species a further even weaker adsorbate site has been observed. It is the dominating species at the smallest preparations. Amorphous aggregates show a larger amount of weakly bound species than do ordered aggregates of the same size. This indicates that an increased ratio of defect states to regular sites with decreasing aggregate size accounts for the occurrence of this weakly adsorbed species.

Substantial dissociation of NO occurs at elevated temperatures >350 K. A disproportionation reaction favours the thermal desorption of N-containing species such as NO, $N_2$ and $N_2O$.[22] No $O_2$ or $NO_2$ has been detected, implying solvation of the remaining oxygen within the palladium. The ratio between the reaction product $N_2$ and undissociated NO increases with increasing aggregate size up to 80 Å for a saturation coverage of NO deposited at 100 K. Again this observation has no match with findings on low index single crystals. It has been reported for stepped surfaces like Pd(112).[22] On stepped surfaces thermally induced population of edge sites initiates dissociation. As aggregates exhibit a large amount of edge sites it can be concluded that the edge sites of the aggregates are particularly important for the thermal dissociation.

UV-laser induced desorption of NO has been studied by means of REMPI to detect desorbing molecules quantum state resolved after excitation with nanosecond laser pulses at 6.4 eV. In contrast to single crystals, desorption of intact NO molecules has been observed for small aggregates of 80 Å and below. The desorption efficiencies increase with decreasing aggregate size by one order of magnitude in the size regime under investigation. For aggregates with a diameter of 80 Å the desorption cross sections are at the detection limit of our experimental set-up. Dominantly a weakly bound species desorbs. Analysis of the rotational temperature of desorbing NO as well as the observation of vibrationally excited NO indicates that the excitation process has to be non-thermal. REMPI data do not show any strong size dependence of rotational distributions, neither for the weakly bound nor for the chemisorbed species, even compared to one another.

For most UV-laser induced processes observed on metals the excitation results from an initial excitation within the substrate with a subsequent charge transfer from substrate to adsorbate. Quantisation effects only occur for rather small metal aggregates (smaller than a few tens of atoms for the naked aggregates). The medium aggregates investigated here have still smaller dimensions than the mean free path of the electrons and have a large number of surface atoms with respect to bulk atoms. Using REMPI, information can be obtained about how much energy is stored in the desorbing molecules. Changes in the lifetimes of electronically excited states and the shapes of the potential energy surfaces as a function of aggregate size would result in changes in the final state distributions.

In view of the strong size dependence of the desorption efficiency changes in the final state distributions with aggregate size are surprisingly small. We can speculate about three different mechanisms:

1. Desorption from low coordinated Pd atoms. One possible explanation is that desorption occurs predominately from defect-like sites (edges, kinks, defects). For such a site the electronic structure is strongly localised and therefore little affected by the overall electronic structure. This would result in similar lifetimes of the excited state and thus similar final state distributions. An increase in desorption efficiency with decreasing aggregate size would therefore be dominated by the amount of such sites available. Particularly small amorphous aggregates with a high degree of defects show efficient desorption. For those aggregates weakly adsorbed species are dominant. Apparently depopulation of defect states is important. IRAS and TPD data also reveal depletion of more strongly bound species for all aggregate sizes. In view of the small difference in final state distributions of the strongly and weakly bound species diffusion is likely to occur. Thermally induced preferential population of weakly bonding sites *via* diffusion from more strongly bound regular adsorption sites has been reported for Pd(112) before.[22] The laser induced process could then be seen as a two step mechanism ((i) laser induced diffusion to weakly interacting adsorption sites after the first laser shot, (ii) desorption from weaker bound species induced by a second laser pulse). A one step process (diffusion followed by collision induced desorption) might contribute to a slow and rotationally cold desorption channel visible in the velocity flux distributions. The latter process leads to a certain thermalisation with the substrate during the residence time before desorption. However, there is one problem with this interpretation: the larger aggregates still exhibit a substantial number of edges and kinks. No weak adsorbate state comparable to the species on amorphous aggregates is detectable in TPD or from temperature dependent IRAS, while the laser induced desorption is still observable but much less efficient.

2. Laser induced spill-over. A second explanation is that laser excitation does not cause desorption at defects of the metal particles but spill-over to the alumina support. This causes an increase in the NO population at alumina defect sites. As is apparent from TPD and REMPI a certain population of NO at defect sites of alumina is possible at 100 K. The increase in desorption efficiency with decreasing aggregate size could thus be explained by shortening of the diffusion paths and thus promotion of the population of the alumina defect sites. The weakly and more strongly bound molecules are likely to have different diffusion barriers which would explain the different efficiency of desorption of the two species. The similar rotational temperatures of NO desorbing from defect states at pure alumina and the alumina modified *via* Pd aggregates within a large range of aggregates would support this hypothesis. The only contradiction is the clear drop within rotational temperatures observed for the largest aggregates.

3. Electronic effects. Desorption has been detected for aggregates below a diameter of 80 Å. Similarities in final state distributions have mainly been detected for aggregates with diameters below 45 Å. The mean free path of electrons in metals is of the same order of magnitude at an excitation energy of 6.4 eV.[35] There is a large number of examples viewed with scanning tunnelling microscopy in which oscillatory local-density-of-states have been documented because of scattering and interference of electrons in low-dimensional metal structures at steps, adsorbates and point defects.[36] Such changes in local density with laser excitation could destabilize the NO–surface bond and thus induce either diffusion or desorption. This hypothesis is supported by the fact that for laser induced desorption and dissociation of methane the lack of the dissociation channel occurs for aggregates around $(36.5 \pm 5.5)$ Å, which is of the same order of magnitude as for the aggregates with similar desorption behaviour of NO.[8]

From the experiments presented none of the above-mentioned processes can be fully ruled out. A full understanding of these experiments will necessitate extensive theoretical calculations.

To summarise, the first quantum state resolved experiments of laser induced desorption from nanoparticulate metal particles recorded as a function of particle size and morphology have revealed a number of intriguing new findings which should stimulate further theoretical as well as experimental investigations. Certainly the number of open questions is still large. The reduction of metals to nanometre dimensions causes more than just a modification of the electronic structure. A number of new phenomena, such as a completely different adsorption behaviour even for aggregates consisting of up to 10 000 atoms, occur. This changed adsorption behaviour seems to be the key for laser induced desorption being detectable for the system under investigation. More has to be done to fully understand the whole complexity of photochemistry of nanosized systems. This should include not only experimental studies on the adsorption behaviour of the strongly repulsive interacting NO on such aggregates or on the probability of spill-over, but also theoretical calculations. There the emphasis should be put, for example, on how the terraces are affected by local density fluctuations at the edges, when adsorption of NO changes the properties of metallic Pd aggregates towards more molecular-like behaviour, whether and under which conditions oscillations in the electron densities within the particle are formed or how relevant surface states vary with aggregate size.

## Acknowledgement

The authors should like to thank Marcus Bäumer, Jörg Libuda and Martin Frank for helpful discussions concerning the preparation and properties of the palladium aggregates. The Deutsche Forschungsgemeinschaft, the Ministerium für Wissenschaft und Forschung des Landes Nordrhein-Westfalen, and the Fonds der chemischen Industrie gave us financial support.

## References

1 H.-J. Freund, *Angew. Chem., Int. Ed. Engl.*, 1997, **36**, 453.
2 C. T. Campbell, *Surf. Sci. Rep.*, 1997, **27**, 1.
3 D. R. Rainer, C. Xu and D. W. Goodman, *J. Mol. Catal. A*, 1997, **119**, 307.
4 C. R. Henry, *Surf. Sci. Rep.*, 1998, **31**, 235.
5 V. P. Zhdanov and B. Kasemo, *Surf. Sci. Lett.*, 1999, **432**, L599.
6 J. W. Gadzuk, *Phys. Rev. Lett.*, 1996, **76**, 4234.
7 J. W. Gadzuk, *J. Electron Spectrosc. Relat. Phenom.*, 1999, **98**, 321.
8 K. Watanabe, Y. Matsumoto, M. Kampling, K. Al-Shamery and H.-J. Freund, *Angew. Chem.*, 1999, **111**, 2328.
9 F. M. Zimmermann and W. Ho, *Surf. Sci. Rep.*, 1995, **22**, 127.
10 F. Budde, T. F. Heinz, M. M. T. Loy, J. A. Misewich, F. de Rougemont and H. Zacharias, *Phys. Rev. Lett.*, 1991, **66**, 3024.
11 M. Menges, B. Baumeister, K. Al-Shamery, H.-J. Freund, C. Fischer and P. Andresen, *Surf. Sci.*, 1994, **316**, 103.
12 T. Itoyama, M. Wilde, M. Matsumoto, T. Okano and K. Fukutani, *Surf. Sci.*, 2001, **493**, 84.
13 M. Bäumer, J. Libuda and H.-J. Freund, in *Chemisorption and Reactivity on Supported Clusters and Thin Films*, ed. R. M. Lambert and G. Pacchioni, Kluwer, Dordrecht, 1997, p. 61.
14 K. H. Hansen, T. Worren, S. Stempel, E. Lægsgaard, M. Bäumer, H.-J. Freund, F. Besenbacher and I. Stensgaard, *Phys. Rev. Lett.*, 1999, **83**, 4120.
15 D. C. Jacobs and R. N. Zare, *J. Chem. Phys.*, 1986, **85**, 5457.
16 H. Conrad, G. Ertl, J. Küppers and E. E. Latta, *Surf. Sci.*, 1977, **65**, 235.
17 H.-D. Schmick and H.-W. Wassmuth, *Surf. Sci.*, 1982, **123**, 471.
18 M. Bertolo and K. Jacobi, *Surf. Sci.*, 1990, **226**, 207.
19 S. W. Jorgensen, N. D. S. Canning and R. J. Madix, *Surf. Sci.*, 1987, **179**, 322.
20 R. Raval, M. A. Harrison, S. Haq and D. A. King, *Surf. Sci.*, 1993, **294**, 10.
21 R. G. Sharpe and M. Bowker, *Surf. Sci.*, 1996, **360**, 21.
22 R. D. Ramsier, Q. Gao, H. Neergard Waltenburg, K.-W. Lee, O. W. Nooij, L. Lefferts and J. T. Yates, Jr., *Surf. Sci.*, 1994, **320**, 209.
23 C. Nyberg and P. Uvdal, *Surf. Sci.*, 1988, **204**, 517.
24 W. A. Brown and D. A. King, *J. Phys. Chem. B*, 2000, **104**, 2578.
25 K. Wolter, O. Seiferth, H. Kuhlenbeck, M. Bäumer and H.-J. Freund, *Surf. Sci.*, 1998, **399**, 190.
26 M. Bertolo, K. Jacobi, S. Nettesheim, M. Wolf and E. Hasselbrink, *Vacuum*, 1990, **41**, 76.
27 M. Bertolo and K. Jacobi, *Surf. Sci.*, 1990, **236**, 143.
28 P. Hollins, *Surf. Sci. Rep.*, 1992, **16**, 51.
29 R. Imbihl, in *Surface Science, Principles and Current Applications*, ed. R. J. MacDonald, E. C. Taglauer and K. R. Wandelt, Springer, Berlin, 1996, p. 203.
30 H. Cordatos, T. Bunluesin and R. J. Gorte, *Surf. Sci.*, 1995, **323**, 219.
31 R. Smoluchowski, *Phys. Rev.*, 1941, **60**, 661.
32 J. Tersoff and L. M. Falicov, *Phys. Rev. B*, 1981, **24**, 754.
33 Y. Hasegawa and Ph. Avouris, *Phys. Rev. Lett.*, 1993, **71**, 1071.
34 M. F. Crommie, C. P. Lutz and D. M. Eigler, *Nature*, 1993, **363**, 524.
35 C. R. Brundle, *Surf Sci.*, 1975, **48**, 99.
36 Ph. Avouris, I.-W. Lyo and P. Molinàs-Mata, in *Electronic Surface and Interface States on Metallic Systems*, ed. E. Bertel and M. Donath, World Scientific, Singapore, 1995, p. 217.